Development of Silicalite-1-encapsulated Ni catalyst from Ni phyllosilicate for dry reforming of methane

Yusheng Zhang
Tokyo Institute of Technology
Ryota Takahashi
Tokyo Institute of Technology
Kentaro Kimura
Tokyo Institute of Technology
Hiroyasu Fujitsuka
Kyoto University
Teruoki Tago (tago.t.aa@m.titech.ac.jp)
Tokyo Institute of Technology

Research Article

Keywords: Ni phyllosilicate, Silicalite-1, Ni@S-1, encapsulation structure, DRM

Posted Date: September 6th, 2022

DOI: https://doi.org/10.21203/rs.3.rs-2017757/v1

Abstract

CO_2 (dry) reforming of methane (DRM) is a significant and useful reaction from the standpoint of effective utilization and conversion of two main greenhouse gases to value-added synthesis gas. To achieve highly efficient and stable DRM reaction, a Silicalite-1-encapsulated ultrafine Ni nanoparticle catalyst(Ni@S-1)by using Ni phyllosilicate (Ni-PS) as precursor was newly developed. This Ni@S-1 catalyst exhibited negligible coke deposition (0.5 wt.%) evaluated at 600°C for 5 h. Additionally, this Ni@S-1 catalyst presented high and stable catalytic performances and maintained the Ni nanoparticles with ultrafine size (< 7 nm) at 850°C for 24 h. Therefore, this Ni@S-1 catalyst showed good suppression of coke formation and high resistance to nickel sintering and thus was promising for DRM reaction.

1 Introduction

Global warming and climate change caused by the emission of greenhouse gases (GHGs) from human activities have become severe issues [1–5]. Given that, dry (CO_2) reforming of methane (DRM, as shown in **Eq. 1**) provides an effective way to efficiently remove and convert two leading greenhouse gases, CH_4 + CO_2, into valuable syngas (i.e., CO and H_2) with a theoretical H_2/CO molar ratio approximately 1[6–8]. This syngas can be used as feedstock to synthesize value-added oxygenated chemicals and long-chain hydrocarbons via Fischer-Tropsch reactions [9–12].

$$CH_4 + CO_2 \longleftrightarrow 2H_2 + 2CO \qquad \Delta_r H^{\circ}_{298K} = +247\ \text{KJ/mol} \qquad \text{Equation 1}$$

The Nickel (Ni) based catalysts have shown high DRM activity, abundant resources, and relatively low cost, so Ni catalysts are believed to be the most promising for DRM reaction [13–17]. However, the traditional Ni-based catalysts cannot meet the industrial application because of their fast deactivation under harsh DRM conditions [9, 18]. According to the thermodynamics calculation in Fig. 1, the coke deposition would be severe when the reaction temperature was below 700°C. On the other hand, the reaction temperature should be higher than 800°C to achieve a high single-pass conversion of CH_4 and CO_2, but the Ni sintering was favorable to occur at such high temperatures [2]. Therefore, it is necessary to develop a highly active and stable Ni-based catalyst with high suppression of coke formation and good resistance to Ni sintering for DRM reaction.

Significant efforts have been devoted to overcoming the problems. It was reported that the nucleation process of the carbon was inhibited over the small Ni particles with a size of < 7 nm [19–21]. That is, carbon deposition could be suppressed by preparing a catalyst with ultrafine Ni particles. Another well-known strategy to restrict coke formation is confining Ni particles in porous materials to get an encapsulation structure since the space in those porous supports for coke deposition was limited[2, 3, 22, 23]. Additionally, it has been confirmed that the porous support-encapsulated Ni catalyst also showed excellent sintering resistance attributed to the spatial confinement effect of the support and/or strong metal-support interaction [24–27]. Given all these, immobilization of ultrafine Ni nanoparticles (NPs)

inside various porous materials, such as SiO_2 [28–31], Al_2O_3 [25, 32], ZrO_2 [24, 33, 34], etc., with core-shell and yolk-shell structure have been proposed and explored. These catalysts showed high DRM activity and good coking-/ sintering-resistant abilities. Notably, as mentioned above, considering the strong endothermicity of the reaction, the DRM reaction generally proceeds at relatively high temperatures (> 800°C) to achieve high efficiency. However, most encapsulated Ni catalysts reported to date suffered from the partial collapse of the porous shell layer at temperatures higher than 800°C due to the presence of water produced by the concurrent reverse water-gas shift reaction (RWGS, **Eq. 2**) in the DRM process. This side effect may lead to the formation of unencapsulated Ni particles and gradual Ni sintering and thus resulting in unrecoverable deactivation. Therefore, encapsulation of Ni NPs inside thermally stable support is essential for application at high temperatures.

$$H_2 + CO_2 \longleftrightarrow H_2O + CO \qquad \Delta_r H^{\circ}_{298\,K} = +41\ \text{KJ/mol} \qquad \text{Equation 2}$$

Featured by the high thermal stability (especially siliceous zeolites such as Silicalite-1), rigid framework, regular channels, and high specific surface area, zeolite has been a better candidate to confine Ni NPs [16, 23, 35, 36]. With these points in mind, our group successfully prepared Silicalite-1-encapsulated Ni catalyst (Ni@S-1) using amorphous silica-encapsulated Ni-oxide ($NiOx@SiO_2$) as the Ni precursor [18]. This $NiOx@SiO_2$ was first formed in the microemulsion solution, followed by adding the powdery $NiOx@SiO_2$ intozeolite mother liquor. After hydrothermal synthesis (HTS), it was confirmed that the needle-like Ni phyllosilicate (Ni-PS) was formed on the primary crystal grain boundary of Silicalite-1 particles (Ni-PS@S-1) and that it was converted to Ni NPs by the reduction process. Thus, the Ni@S-1 catalyst exhibited high DRM activity with excellent inhibition ability for carbon deposition and high thermal stability due to the immobilization of ultrafine Ni particles within the Silicalite-1.

Ni-PS was reportedly synthesized under hydrothermal conditions in an alkaline solution [16, 37–40], and as described above, the formation of needle-like Ni-PS was observed within Silicailte-1 after HTS. Hence, we developed a new preparation method for encapsulated catalysts using Ni-PS as a Ni source.

Herein, to achieve highly efficient and stable conversion of CH_4 and CO_2 to syngas by DRM reaction, we developed Silicalite-1-encapsulated Ni catalyst (Ni@S-1) by a new method, in which direct addition of Ni-PS as Ni source into the zeolite mother liquid, followed by hydrothermal synthesis (HTS). The Ni-PS was confined within the S-1 particle, and ultrafine Ni particles were successfully formed in the inter-crystalline pore of the S-1 particle after reduction (Ni@S-1). In this research, we proposed a new method for preparing encapsulated catalyst and demonstrated the high suppression of coke deposition, good resistance to Ni sintering, and extended durability for DRM reaction over the Ni@S-1 catalyst.

2 Experimental

2.1 Chemicals

Nickel (II) nitrate hexahydrate ($Ni(NO_3)_2.6H_2O$, > 99%), ammonia solution (> 28 wt.%), tetraethyl orthosilicate (TEOS, > 95.0%,), tetrapropylammonium hydroxide aqueous solution (TPAOH, 10% in H_2O), and distilled water were purchased from

FUJIFILM Wako Pure Chemical Industries, Ltd., Japan. In this study, all chemicals were purchased commercially without further purification. Distilled water was used throughout the experiment.

2.2 Catalyst Preparation

The phyllosilicate-derived Ni@S-1 catalyst was prepared in two steps. Firstly, 3 wt.% Ni-PS was prepared by hydrothermal synthesis (HTS) method as follows: preparation of nickel ammonia complex solution ($Ni[NH_3]_6)^{2+}$) by adding calculated amounts of 1M of nickel nitrate aqueous solution to diluted ammonia solution. Then, the Si source (TEOS) was added to the prepared nickel ammonia complex solution. After stirring and hydrolysis of TEOS for 2 h. The resulting mixture was transferred into a Teflon-lined autoclave reactor and hydrothermally treated in a tumbling oven at 100°C for 72 h. After HTS, the Ni-PS powder was obtained by centrifugal treatment, washed with distilled water three times, and dried overnight at 110°C, followed by calcination in air at 550°C for 12 h.

Then, the Silicalite-1-encapsulated Ni nanoparticle catalyst with nominal Ni loading of 1 wt.%. (Ni@S-1) was prepared by using the obtained Ni-PS powder as the Ni source. First, the TEOS, TPAOH, and distilled water with a molar composition of SiO_2: TPAOH: H_2O (1: 0.33: 50) were mixed and stirred overnight to form homogenous zeolite mother liquors. Then, the as-synthesized 3 wt.% Ni-PS was added to zeolite mother liquor and stirred for another 6 h. The resultant slurry was moved to a 100 mL Teflon-lined autoclave and was hydrothermally treated at 100°C for 72 h. After the second HTS treatment, the solid product was collected by centrifugation, washed with distilled water three times, and dried at 110°C overnight. Finally, the prepared sample was calcined in a muffle furnace at 550°C for 12 h to remove the organic template.

For comparison, two reference catalysts were prepared. At first, the 1wt.% Ni-PS (donated as Ni-PS) was prepared by the same procedures as the preparation of Ni-PS mentioned above. Another sample was prepared by the conventional impregnation method with theoretical Ni loading of 1 wt.% supported both on the surface and inside of Silicalite-1 zeolite. The Silicalite-1 support for the Ni/S-1 catalyst was prepared using the same molar compositions of SiO_2, TPAOH, and distilled water for Ni@S-1 preparation. However, the hydrothermal temperature was set at 180°C to get a Silicalite-1 zeolite with high crystallinity and fewer defects. Then, the as-prepared Silicalite-1 zeolite was impregnated with the $Ni(NO_3)_2.6H_2O$ solution dissolved in ethanol. Then, the obtained mixture was stirred with a glass rod for 30 min, evaporated at room temperature overnight and dried at 110°C for 3 h. Finally, the obtained solid was calcined in a muffle furnace at 550°C for 12 h. The resulting sample was denoted as Ni/S-1.

2.3 Catalyst Characterization

The Ni loading of the as-synthesized samples was detected by X-ray fluorescence (XRF, Supermini, Rigaku Co., Ltd., Japan). The crystallinity and phase identification were evaluated using X-ray diffraction (XRD, SmartLab, Rigaku Co., Ltd., Japan) with Cu Kα radiation (λ = 0.154 nm), operating at 30 kV and 10 mA, a scanning rate of 4°/min, and a step size of 0.02°. Diffraction peaks were recorded in a 2θ range of 5–60°.

The morphology of the samples was observed by a field-emission scanning electron microscope (FE-SEM, S-5200, Hitachi Ltd., Japan) with an acceleration voltage of 1 kV. The shape and size of the Ni species in the prepared samples were observed using a field-emission transmission electron microscope (FE-TEM, H-7650 Zero A, Hitachi Ltd., Japan) operated at an acceleration voltage of 120 kV.

The porosity of the catalysts was studied via the nitrogen adsorption-desorption isotherms (BELSORP mini X, Microtrac MRB, USA) at 77 K. The specific surface area was analyzed using Brunauer-Emmett-Teller (BET) method. The micropore volume was calculated based on the t-plot method.

The redox property of the samples was measured by H_2-temperature programmed reduction (H_2-TPR). The measurement was carried out using a fixed-bed reactor equipped with a mass spectrometer (BELMASS, MicrotracBEL, Inc., Japan). Typically, 0.4 g of the shaped sample was precalcined in the air at 400°C for 1 h and then cooled down in Ar stream to 100°C. After the temperature was maintained for 90 min, the gas stream was switched to 5% H_2/Ar gas. Subsequently, the sample was heated from 100 to 900°C at a ramping rate of 10°C/min and then held there for 1 h. The hydrogen consumption and reduction temperature of the Ni species were estimated by the decrease in the intensity of m/z = 2 of the mass spectrometer.

Finally, the amount of carbon deposition on the spent catalysts was analyzed by the Thermogravimetric analysis (TG-DTA, TG 8120, Rigaku Co., Ltd., Japan). The spent catalyst sample was heated in the air (100 mL/min) at a ramp rate of 10°C/min to 900°C and kept at 900°C for 1 h.

2.4 Catalytic Performance Evaluation

The catalytic activity and stability of the prepared catalysts for DRM reaction were evaluated in a down-flow fixed bed reactor under atmospheric pressure. In detail, 270 mg of the pelleted catalyst (300–600μm) was packed into a quartz tube reactor and then reduced in 60 mL/min of 50 vol.% H_2/N_2 at 850°C for 1 h. Subsequently, adjusting the system to the targeted reaction temperature in the N_2 stream and then feeding 80 mL/min of the reaction gas (CH_4: CO_2: Ar = 20: 20:40 mL/min) and 10 mL/min of He gas (functioned as internal standard gas) into the reactor. The coking suppression ability of the catalyst was measured at 600°C and GHSV of 20,000 mL/g/h. The sintering resistance and durability of the catalyst were assessed at 850°C and GHSV of 20,000 or 400,000 mL/g/h with different durations. The GHSV value was adjusted by diluting the catalyst with blank Silicalite-1 or SiO_2 to change the absolute amount of catalyst loaded into the reactor.

The effluent gases analysis was carried out using online gas chromatographs (GC-8A, Shimadzu Co., Ltd., Japan) equipped with an active carbon column connected to a thermal conductivity detector (TCD). The CH_4, CO_2, H_2, CO, and He gases were detected in all the experiments. The conversion of methane (X_{CH4}), CO_2 (X_{CO2}), the H_2/CO molar ratio, and carbon balance were defined as follows:

$$X_{CH4}\ (\%) = (1 - F_{CH4,out}/\ F_{CH4,in}) \times 100\%$$

$$X_{CO2}\ (\%) = (1 - F_{CO2,out}/\ F_{CO2,in}) \times 100\%$$

$$H_2/CO = F_{H2-out}/\ F_{CO-out}$$

$$\text{Carbon balance}\ (\%) = F_{CO-out}/\ (F_{CH4,in}-F_{CH4,out}+ F_{CO2-in}- F_{CO2-out}) \times 100\%$$

where $F_{i,\ in}$ and $F_{i,\ out}$ are the inlet and outlet flow rates of component i, respectively.

3. Results And Discussion

3.1 Characterization of the as-prepared samples

Several characterization techniques were performed to confirm whether the preparation of the Ni-PS by the HTS method was feasible and successful. As shown in Fig. S1, the needle-like Ni-PS with strong metal-support interaction was successfully synthesized. Then, the obtained 3 wt.% Ni-PS powder was added to zeolite mother liquor as the Ni source to prepare the Ni@S-1 catalyst.

Then, the as-prepared catalysts were characterized. As indicated by the XRD patterns in Fig. 2, Ni@S-1 and Ni/S-1 exhibit characteristic diffraction peaks corresponding to Silicalite-1 zeolite (JCPDS 44–0696), suggesting the well-crystallized MFI zeolite was synthesized. On the contrary, the diffraction pattern of reference Ni-PS has only a very broad peak and no peaks indicative of crystalline phases, indicating the presence of fully amorphous SiO_2. Notably, no NiO or other Ni species were detected by XRD observed over all the three samples because of its lower loading content and good dispersion of the very small NiO particles. As shown in Fig. 2(b), there were no distinct differences in peak position and intensity of XRD patterns before and after H_2 reduction, showing the high thermal stability of the Silicate-1 zeolite. Besides, the characteristic peak of metallic Ni or other Ni species were not found in all the catalysts, identifying the formation of ultrafine and highly dispersed Ni NPs in each catalyst. These results were also evidenced by SEM observation in Fig. S2. The Ni@S-1 and Ni/S-1 catalysts showed typical morphology of MFI zeolite. For comparison, the Ni-PS exhibited totally irregular and randomly distributed shape, which is consistent with that typically observed for amorphous silica.

Table 1 lists the Ni loading of the samples measured by XRF. All the three samples exhibited comparable Ni loading to the nominal value. Hence, most Ni atoms were recovered during the preparation. Figure 3 presents the nitrogen adsorption–desorption isotherms of the samples after H_2 reduction, and the associated BET surface area and micropore volume results are summarized in Table 1. Ni@S-1 with S_{BET}

= 459 m^2/g and V_{micro}.= 0.12 cm^3/g and Ni/S-1 with S_{BET} = 441 m^2/g and V_{micro}.= 0.18 cm^3/g exhibited the typical type I isotherms for microporous materials, indicating that the significant micropores were developed in these catalysts. In contrast, a relatively small N_2 uptake in the micropore filling stage was observed for Ni-PS, verifying that the Ni-PS sample contained a smaller number of micropore with a surface area of 137.6 m^2/g and micropore volume of only 0.01 cm^3/g. From the results of XRD and N_2 adsorption measurements, we can conclude that the Ni@S-1 with Silicalite-1 structure using Ni-PS as Ni source was successfully prepared.

Table 1
Properties of the prepared catalysts after H_2 reduction at 850°C for 1 h

	Ni@S-1	Ni/S-1	Ni-PS
Ni loading measure by XRF (wt.%)	0.99	1.02	0.97
BET surface area (m^2/g)	459.3	440.5	137.6
Micropore volume (cm^3/g)	0.119	0.180	0.01

Next, the H_2-TPR analysis was performed. Figure 4 depicts the hydrogen consumption as a function of temperature during the process of H_2-TPR. As the temperature increased, for Ni/S-1 catalyst, a major and broad reduction peak ranging from 400 to 650°C (peaked at ca. 560°C) should be attributed to the reduction of NiO supported on the outer surface of Siliclaite-1 zeolite with weak interaction. Meanwhile, a minor peak at 700–900°C was associated with NiO introduced into the zeolite channels with improved interaction [18]. In contrast, the large reduction peak at 600–900°C for NiO@S-1 and NiO-PS was assigned to the reduction of Ni-PS to metallic Ni [41]. This illustrated the formation of Ni-PS in Ni@S-1. Based on the findings above, the Ni species immobilized in Silicalite-1 showed strong metal-support interaction in comparison with the NiO deposited on the external surface of Silicalite-1 zeolite.

Then, after reduction by H_2 at 850^oC for 1 h, the TEM observations were undertaken to check the morphology and distribution of Ni particles. As presented in Fig. 5(a)-(b), ultrafine Ni NPs in the Ni@S-1 sample were uniformly and well distributed over the S-1 host and had a narrow size distribution from 1 to 8 nm and average diameter of 2.9 nm, which is the expected size of Ni (< 7nm). This demonstrates that the Ni NPs should be embedded in the Silicalite-1 crystal and hence showing good anti-sintering ability. By contrast, as can be seen from Fig. 7(c)-(d), Ni NPs with wider size distribution from 2 to 16 nm and with a larger mean size of 4.9 nm were detected for Ni/S-1, suggesting the agglomeration of Ni particles situated on the surface of the Si-1 zeolite occurred in H_2 stream. For sample from Ni-PS, Ni NPs were 4.3 nm in mean size and moderately distributed over the amorphous silica. The narrower size distribution of

Ni NPs in Ni-PS compared to that of Ni/S-1 thanks to the stronger interaction between Ni species and silica of the phyllosilicate structure.

On the basis of the characterization results, we concluded that adding Ni-PS as Ni source to zeolite mother liquor, the Ni-PS was successfully anchored in Silicalite-1 crystal after HTS. Then, ultrafine Ni NPs could be formed and encapsulated in Silicalite-1 after H_2 reduction.

3.2. Evaluation of coking suppression for DRM at 600 °C

The anti-coking performance of Ni@S-1, Ni/S-1, and Ni-PS samples in DRM reaction was evaluated at 600°C, where coke formation was preferable and speedy according to the calculation of thermodynamics. Before the reaction, the catalysts were pre-treated in hydrogen at 850°C for 1 h. Notably, the dashed lines plotted in Fig. 6 represent the thermodynamic equilibrium values estimated by the assumption that the DRM and concurrent RWGS reached equilibrium without coke formation. As shown in Fig. 6, Ni@S-1 and Ni-PS catalysts reached the thermodynamic equilibrium for CH_4 conversion, CO_2 conversion, and H_2/CO ratio and maintained their activity for 5 h, and the carbon balance for them was kept at ca. 100% during the reaction. All these imply that Ni@S-1 and Ni-PS exhibited high DRM activity and excellent ability for suppression of coke formation. Comparatively, the Ni/S-1 catalyst exhibited comparable CH_4 conversion, but lower CO_2 conversion, higher H_2/CO ratio, and lower carbon recovery in gaseous products than that of the former two catalysts, indicating that the side coke formation reactions, e.g., methane decomposition (Eq. 3) [42] and/or the CO disproportionation reaction (Eq. 4) [43], were promoted over Ni/S-1 catalyst.

$$CH_4 \longleftrightarrow C\ (coke) + H_2 \qquad \Delta_r H^{\circ}_{298\,K} = +75\ KJ/mol \qquad \text{Equation 3}$$

$$2CO \longleftrightarrow C\ (coke) + CO_2 \qquad \Delta_r H^{\circ}_{298\,K} = -171\ KJ/mol \qquad \text{Equation 4}$$

Next, TG measurement was employed to calculate the amount of coke deposited after DRM reaction. As listed in inset of Fig. 6d and Fig. S3, the accumulated coke contents were 0.5 wt.% for Ni@S-1, whilst it was 40.9 wt.% for Ni/S-1.

Then, the morphology of the spent catalysts observed by SEM and TEM was carried out to confirm the coke accumulation. Figure 7 shows that negligible carbon species were observed on the spent Ni@S-1 and Ni-PS catalysts, whereas numerous filamentous carbons were found on the spent Ni/S-1 catalyst. These results coincide well with the results from the catalytic performances.

From these results, we can conclude that most of the Ni NPs of Ni@S-1 catalyst should be confined inside of the support, thus resulting in the internal space around the Ni NPs for coke deposition was limited and preventing the aggregation of the Ni particles. Therefore, the Ni catalysts with encapsulation structure could effectively inhibit coke formation. Contrarily, for the Ni/S-1 catalyst, relatively more Ni particles were located and exposed on the external surface of Silicalite-1with weak interaction, so the

agglomeration of the Ni NPs easily occurred and tended to form larger particles. Consequently, the large amount of carbon was favorable to grow on its surface, manifesting the Ni/S-1 prepared by the conventional impregnation method was not suitable for industrial application. As for Ni-PS catalyst, the coke content was 0.9 wt.%, the good suppression of coke formation of the Ni–PS catalyst may be due to the strong metal-support interaction of phyllosilicate material that gives rise to Ni sintering resistance to form large Ni particle at moderate temperature, thus showing its suppression towards coking[41, 44].

3.3. Evaluation of thermal stability for DRM at 850^{o}C

Then, the Ni@S-1 and Ni-PS catalysts were further evaluated at 850^{o}C to investigate their resistance to Ni sintering and thermal stability. Not surprisingly, both catalysts reached thermodynamic equilibrium in Fig. 8 due to the high reaction temperature and low GHSV employed, and hence the active sites and residence time are enough to achieve equilibrium values.

More importantly, as shown in Fig. 9, the Ni NPs in the spent Ni@S-1 catalyst after reaction at 850^{o}C for 5 h were still well dispersed and the average size slightly increased to 4.3 nm in Fig. 9b. In contrast, the Ni-PS sample suffered from severe sintering, the average size of nickel particles dramatically increased to ca. 8.3 nm after reaction (Fig. 9d), and several nickel particles with diameters greater than 10 nm were detected. Combined with the N_2 adsorption and XRD measurements in Fig. S4 and Table S1, such discrepancy revealed that Silicalite-1 exhibited high thermal stability and the Ni nanoparticles confined in Silicalite-1 zeolite possessed good resistance to sintering. Contrarily, the structure of amorphous silica in Ni-PS collapsed and then the serious Ni sintering occurred.

Finally, the longevity experiments over Ni@S-1 and Ni-PS catalysts were conducted at 850°C and GHSV of 400,000 mL/(g-cat·h) to clear distinguish and examine the intrinsic activity, stability and durability under severe conditions. As displayed in Fig. 10, Ni-PS showed lower initial activity than that of the Ni@S-1 owing to the larger Ni particle and less active sites in this catalyst. Furthermore, the quick deactivation with the reaction time was detected for Ni-PS. The CH_4 conversion, CO_2 conversion, and H_2/CO ratio declined significantly from 81.0%, 88.5%, and 0.89 to 73.8%, 83.6%, and 0.85, respectively, which verified the poor stability of the Ni-PS at high reaction temperature. Comparatively, the initial conversions of CH_4 and CO_2 and products yield over Ni@S-1 catalyst almost reached to thermodynamic equilibrium values even at such high GHSV, identifying its superior catalytic activity due to the presence of highly dispersed ultrafine Ni NPs. After running for 24 h, the CH_4 and CO_2 conversions slightly reduced from 93.4–85.2% and 97.0–92.7%, respectively, illuminating the relatively stable performance of the Ni@S-1 catalyst. Therefore, the Ni@S-1 could produce and maintain ultrafine Ni NPs during DRM due to the encapsulation structure and high thermal stability of the zeolite support.

4 Conclusions

A new and facile strategy to prepare Ni@S-1 catalyst with encapsulation structure and ultrafine Ni nanoparticles was successfully developed, in which the Ni phyllosilicate was synthesized and added to

zeolite mother liquor as Ni source. The TEM, H_2-TPR, and XRD measurement results verified that the Ni phyllosilicate was embedded inside the Silicalite-1 zeolite after hydrothermal synthesis, leading to the formation of highly dispersed Ni nanoparticles with the average size of 2.9 nm confined in the Silicalite-1 zeolite after H_2 reduction. This Ni@S-1 catalyst reached thermodynamic equilibrium activities and showed negligible coke deposition of 0.5 wt.% at 600°C for 5 h after DRM reaction. Moreover, the encapsulation structure and high thermal stability of the Silicalite-1 support enabled Ni@S-1 to restrict the migration and aggregation of Ni NPs and thus keeping the ultrafine Ni NPs (< 7 nm) and exhibiting rather high and stable catalytic performances at 850°C for 24 h. Therefore, the Ni@S-1 using Ni-PS as Ni source showed high suppression of coke formation and good resistance to Ni sintering due to the formation and maintenance of ultrafine Ni nanoparticles in thermally stable Silicalite-1 zeolite support.

Declarations

Conflict of interest There are no conflicts to declare.

Author Contributions

Yusheng Zhang: Conceptualization, Methodology, Formal analysis and investigation, Writing - original draft preparation

Ryota Takahashi: Conceptualization, Methodology, Formal analysis and investigation

Kentaro Kimura: Conceptualization, Methodology, Writing - review and editing, Supervision

Hiroyasu Fujitsuka: Conceptualization, Methodology, Supervision

Teruoki Tago: Conceptualization, Methodology, Writing - review and editing, Funding acquisition, Supervision

Acknowledgement

This work was partly supported by Grants in Aid for Scientific Research (B) (21H01700) and JST under STCORP program (JPMJSC2101). Mr. Zhang also appreciates the financial support of China Scholarship Council (No. 202108050037). The authors would also like to acknowledge Materials Analysis Division, Open Facility Center of Tokyo Institute of Technology for the TEM equipment and analysis.

References

1. S. Kim, J. Lauterbach, E. Sasmaz, ACS Catal. 11 (2021) 8247.
2. Y. Liu, Y. Chen, Z. Gao, X. Zhang, L. Zhang, M. Wang, B. Chen, Y. Diao, Y. Li, D. Xiao, X. Wang, D. Ma, C. Shi, Appl. Catal. B. 307 (2022) 121202.
3. Y. Gao, Y. Wei, W. Sun, G. Zhao, Y. Liu, Y. Lu, Fuel. 320 (2022) 123892.

4. I. v. Yentekakis, P. Panagiotopoulou, G. Artemakis, Appl. Catal. B. 296 (2021) 120210.
5. H.S. Roh, K.W. Jun, Catal. Surv. Asia. 12 (2008) 239.
6. J.M. Ginsburg, J. Piña, T. el Solh, H.I. de Lasa, Ind. Eng. Chem. Res. 44 (2005) 4846.
7. T. Kobayashi, T. Furuya, H. Fujitsuka, T. Tago, Chem. Eng. J. 377 (2019) 120203.
8. H. Wang, S. Kim, E. Sasmaz, Chem. Eng. J. 450 (2022) 138111.
9. S. Xu, T.J.A. Slater, H. Huang, Y. Zhou, Y. Jiao, C.M.A. Parlett, S. Guan, S. Chansai, S. Xu, X. Wang, C. Hardacre, X. Fan, Chem. Eng. J. 446 (2022) 137439.
10. F. Wang, L. Xu, W. Shi, J. CO2 Util. 16 (2016) 318
11. M. Zahedi nezhad, S. Rowshanzamir, M.H. Eikani, Int. J. Hydrogen Energy. 34 (2009) 1292.
12. J.S. Kang, D.H. Kim, S.D. Lee, S.I. Hong, D.J. Moon, Appl. Catal. A Gen. 332 (2007) 153.
13. Z. Bian, S. Das, M.H. Wai, P. Hongmanorom, S. Kawi, ChemPhysChem. 18 (2017) 3117.
14. M. Akri, S. Zhao, X. Li, K. Zang, A.F. Lee, M.A. Isaacs, W. Xi, Y. Gangarajula, J. Luo, Y. Ren, Y.-T. Cui, L. Li, Y. Su, X. Pan, W. Wen, Y. Pan, K. Wilson, L. Li, B. Qiao, H. Ishii, Y.-F. Liao, A. Wang, X. Wang, T. Zhang, Nat. Commun. 10 (2019) 5181.
15. S. Kweon, Y.W. Kim, C.H. Shin, M.B. Park, H.K. Min, Chem. Eng. J. 431 (2022) 133364.
16. Y. Lu, D. Guo, Y. Zhao, P.S. Moyo, Y. Zhao, S. Wang, X. Ma, Microporous and Mesoporous Mater. 313 (2021) 110842.
17. Q. Song, R. Ran, D. Li, B. Zhao, D. Weng, Catal. Surv. Asia.. 25 (2021) 312.
18. H. Fujitsuka, T. Kobayashi, T. Tago, J. CO2 Util. 53 (2021) 101707.
19. D. Baudouin, U. Rodemerck, F. Krumeich, A. de Mallmann, K.C. Szeto, H. Ménard, L. Veyre, J.P. Candy, P.B. Webb, C. Thieuleux, C. Copéret, J. Catal. 297 (2013) 27.
20. J.H. Kim, D.J. Suh, T.J. Park, K.L. Kim, Appl. Catal. A Gen. 197 (2000) 191–200.
21. H.S. Bengaard, J.K. Nørskov, J. Sehested, B.S. Clausen, L.P. Nielsen, A.M. Molenbroek, J.R. Rostrup-Nielsen, J. Catal. 209 (2002) 365.
22. M. Kosari, S. Askari, A.M. Seayad, S. Xi, S. Kawi, A. Borgna, H.C. Zeng, Appl. Catal. B. 310 (2022) 121360.
23. B. Gray, J.N. Kuhn, B. Joseph, Chem. Eng. J. 437 (2022) 135353.
24. R.D. binti Rosdin, M. Yusuf, B. Abdullah, Mater. Lett: X. 12 (2021) 100095.
25. Z. Shang, S. Li, L. Li, G. Liu, X. Liang, Appl. Catal. B. 201 (2017) 302.
26. D. Kang, H.S. Lim, J.W. Lee, Int. J. Hydrogen Energy. 42 (2017) 11270.
27. K.S. Park, J.M. Cho, Y.M. Park, J.H. Kwon, J.S. Yu, H.E. Jeong, J.W. Choung, J.W. Bae, Catal. Today. 388–389 (2022) 224.
28. J. Tian, B. Ma, S. Bu, Q. Yuan, C. Zhao, Chem. Comm. 54 (2018) 13993.
29. Z. Li, S. Das, P. Hongmanorom, N. Dewangan, M.H. Wai, S. Kawi, Catal. Sci. Technol. 8 (2018) 2763.
30. S. Das, J. Ashok, Z. Bian, N. Dewangan, M.H. Wai, Y. Du, A. Borgna, K. Hidajat, S. Kawi, Appl. Catal. B. 230 (2018) 220.

31. Z. Bian, S. Kawi, S, ChemCatChem. 10 (2018) 320.
32. J.W. Han, J.S. Park, M.S. Choi, H. Lee, Appl. Catal. B. 203 (2017) 625.
33. M. Zhang, J. Zhang, Y. Wu, J. Pan, Q. Zhang, Y. Tan, Y. Han, Appl. Catal. B. 244 (2019) 427.
34. M. Meiliefiana, T. Nakayashiki, E. Yamamoto, K. Hayashi, M. Ohtani, K. Kobiro, Nanoscale Res. Lett. 17 (2022) 1.
35. H.K. Min, S. Kweon, Y.W. Kim, H. An, D. Jo, E.D. Park, C.H. Shin, M.B. Park, Appl. Catal. B. 298 (2021) 120627.
36. J. Wang, Y. Fu, W. Kong, F. Jin, J. Bai, J. Zhang, Y. Sun, Appl. Catal. B. 282 (2021).
37. B. Ma, H. Cui, C. Zhao, Chem. Comm. 53 (2017) 10358–10361.
38. T. Wu, Q. Zhang, W. Cai, P. Zhang, X. Song, Z. Sun, L. Gao, Appl. Catal. A Gen. 503 (2015) 94.
39. Y.Y. Chen, Y.C. Chang, W.Y. Hung, H.P. Lin, H.Y. Shih, W.A. Xie, S.N. Li, C.H. Hsu, Int. J. Energy Res. 44 (2020) 9748.
40. M. V Sivaiah, S. Petit, M.F. Beaufort, D. Eyidi, J. Barrault, C. Batiot-Dupeyrat, S. Valange, Microporous and Mesoporous Mater. 140 (2011) 69.
41. M. V. Sivaiah, S. Petit, J. Barrault, C. Batiot-Dupeyrat, S. Valange, Catal. Today. 157 (2010) 397.
42. R. Franz, F.D. Tichelaar, E.A. Uslamin, E.A. Pidko, Appl. Catal. A Gen. 612 (2021) 117987.
43. H. Er-rbib, C. Bouallou, F. Werkoff, Chem. Eng. Trans. 29 (2012) 163.
44. Z. Bian, Z. Li, J. Ashok, S. Kawi, Chem. Comm. 51 (2015) 16324.

Figures

Figure 1

The thermodynamic calculation of DRM reaction. (Reaction conditions: CH_4: CO_2: Ar = 2: 2: 5, 1 bar)

Figure 2

XRD patterns of the as-prepared catalysts: (a) after calcination at 550°C for 12 h and (b) after H_2 reduction at 850°C for 1 h

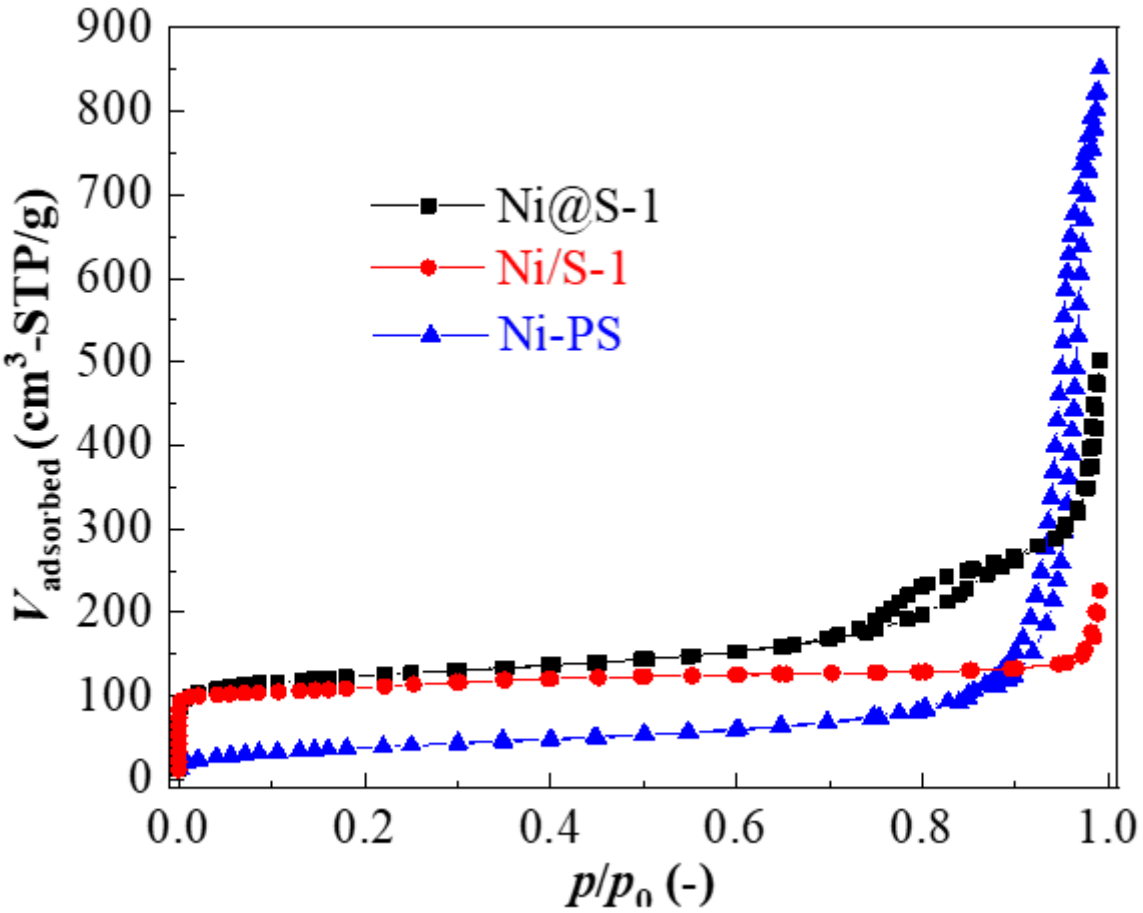

Figure 3

N_2 adsorption isotherms of the as-prepared catalysts after H_2 reduction at 850°C for 1 h.

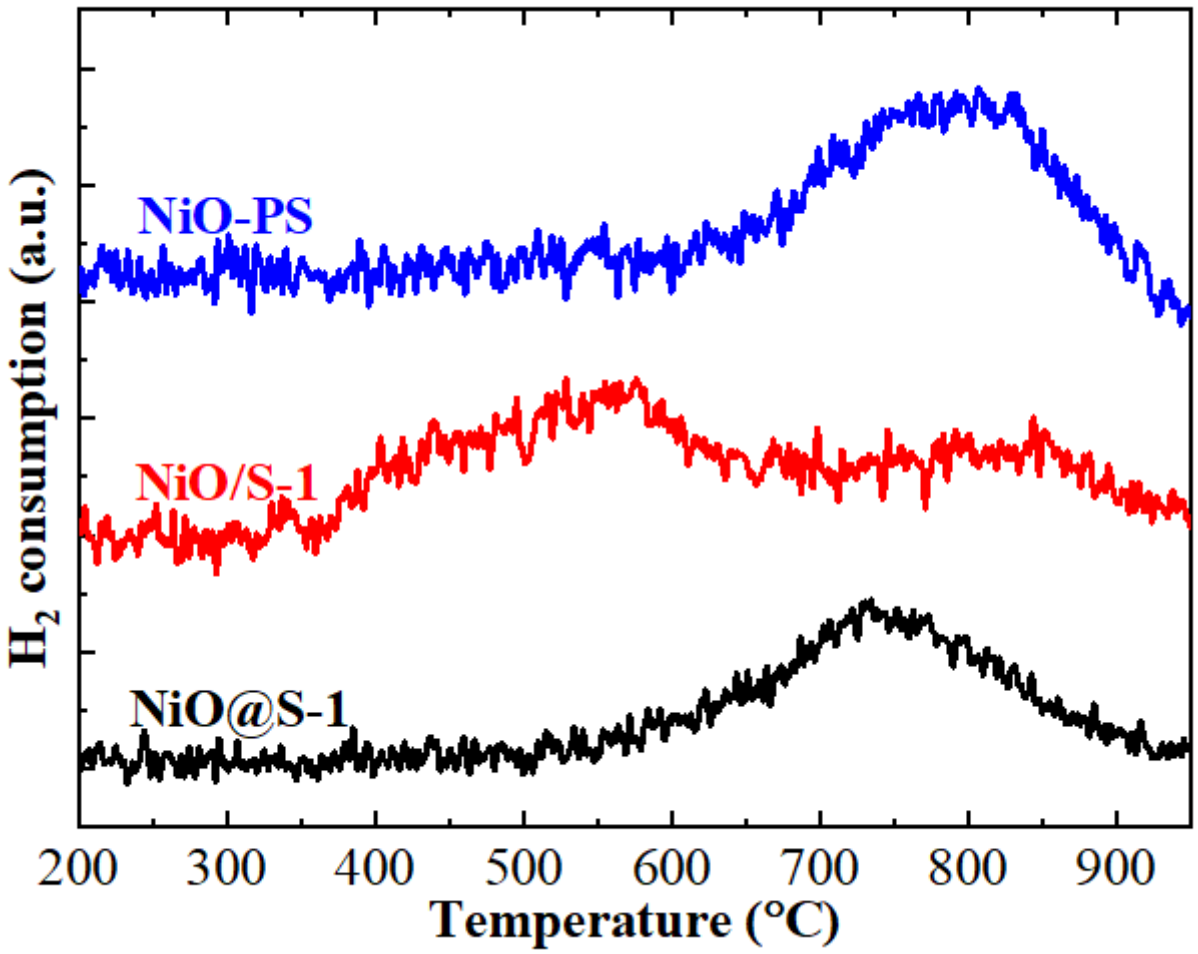

Figure 4

H_2-TPR profiles of the as-prepared catalysts

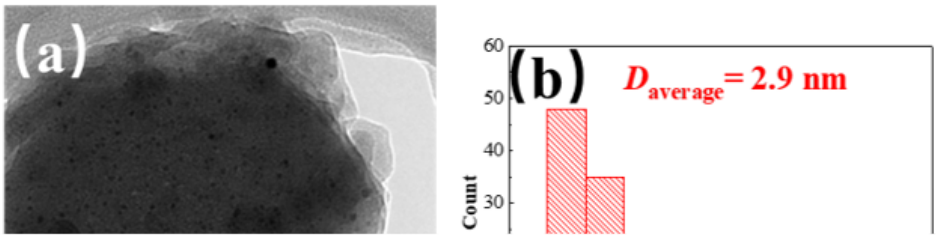

Figure 5

TEM images and corresponding Ni particle size distribution of (a–b) Ni@S-1, (c–d) Ni/S-1, and (e–f) Ni-PS after H_2 reduction at 850°C for 1 h.

Figure 6

Catalytic performances of the as-prepared catalysts for DRM reaction at 600 ^{o}C as function of time on stream: (a) CH_4 conversion, (b) CO_2 conversion, (c) H_2/CO ratio, and (d) carbon balance and correspongding coke content after reaction in inset (reaction conditions: T = 600 ^{o}C, 1 bar, CH_4/CO_2/Ar/ He = 20/20/40/10mL/min, GHSV=20,000mL/(g-cat·h))

Figure 7

SEM (a1-c1) and TEM (a2-c2) images of spent catalysts after DRM reaction at 600 ^{o}C for 5 h: (a) Ni@S-1, (b) Ni/S-1, and (c) Ni-PS.

Figure 8

Catalytic performances of the as-prepared catalysts in DRM reaction at 850 ^{o}C as function of time on stream: (a) CH_4 conversion, (b) CO_2 conversion, (c) H_2/CO ratio, and (d) carbon balance (reaction conditions: T = 850 ^{o}C, 1 bar, CH_4/CO_2/Ar/ He = 20/20/40/10mL/min, GHSV=20,000 mL/(g-cat·h))

Figure 9

TEM images and corresponding Ni particle size distribution of (a–b) Ni@S-1 and (c–d) Ni-PS after DRM reaction at 850°C for 5 h.

Figure 10

Catalytic performances of the as-prepared catalysts in DRM reaction at 850 ^{o}C as function of time on stream: (a) CH_4 conversion, (b) CO_2 conversion, (c) H_2/CO ratio, and (d) carbon balance (reaction conditions: T = 850 ^{o}C, 1 bar, CH_4/CO_2/Ar/ He = 20/20/40/10mL/min, GHSV = 400,000 mL/(g-cat·h)) [Catalysts were diluted with blank support, e.g. blank Silicalite-1 for Ni@S-1 and blank amorphous silica for Ni-PS, to decrease the catalyst amount.]

Supplementary Files

This is a list of supplementary files associated with this preprint. Click to download.

- Supplementarymaterials.docx